Normalization in 3D PET: Comparison of Detector Efficiencies Obtained from Uniform Planar and Cylindrical Sources

T.R.Oakes, V.Sossi, and T.J.Ruth
University of British Columbia/TRIUMF PET Centre
4004 Wesbrook Mall, Vancouver, B.C. V6T 2A3 Canada

Abstract

We have performed a comparison between 3D PET Normalization Factors (NFs) obtained from a uniform planar source and a uniform cylindrical phantom. The NFs have geometric and detector efficiency components. Detector efficiency data were measured using both phantoms. Both efficiency data sets were corrected using geometric factors obtained from a low-scattering planar distribution. NFs derived from 3D planar and 3D cylindrical efficiency data were applied to the sinogram data, yielding axial uniformity indices of 0.78% (2D), 1.71% (3D planar), and 3.40% (3D cylinder), and respective radial uniformity indices of 2.00%, 4.81%, and 4.07%. Correcting the cylinder for scatter prior to calculating the detector efficiencies was found to slightly improve axial uniformity and to slightly degrade radial uniformity. The uniformity obtained from cylinder-derived detector efficiencies is nearly identical to that obtained from plane-source derived efficiencies; the predominant influence on the accuracy of the normalization is the geometric factors used to correct the detector efficiency data.

I. INTRODUCTION

We previously developed a method [1],[2] for calculating Normalization Factors (NFs) for PET studies acquired in 3D (septa removed) mode. This method utilizes a low-scatter planar distribution of radioactivity for the normalization scan source. A set of Geometric Factors (GFs) is calculated from a high-statistics planar-source data set. The GFs are used to correct individual Lines-of-Response (LORs) for variations due to their geometric position relative to other LORs. When a new normalization is required, the planar-source is scanned to determine the individual detector efficiency factors (ε) by creating a three-dimensional fan-beam of LORs associated with each detector [3],[1]. All ε are corrected for geometric variations using the previously calculated GFs to yield the NFs. For each LOR a NF is calculated as follows:

$$NF\left(R_A, R_B, D_i, D_j\right) = \frac{\varepsilon\left(R_A, D_i\right)\varepsilon\left(R_B, D_j\right)}{GF\left(R_A, R_B, D_i, D_j\right)} \qquad (1)$$

where R_A, R_B designate the two detector rings for each LOR and D_i, D_j designate the positions of the two detectors within their respective rings for each LOR.

A plane-source is regarded as the most favorable geometry due to the low level of scattered photons, but is impractical to implement on a routine basis. We have modified this method to use a uniform cylindrical phantom to measure the detector efficiency factors ε. The present comparison of ε obtained from cylindrical and planar sources was initiated to determine if a cylindrical phantom could yield results comparable to a planar source. Other workers have reported on 3D PET normalization using either a cylinder source [4],[5] or a planar source [6],[2] to estimate ε. Kinahan et al. [7] reported that for a component-based normalization method the image uniformity of a uniform cylinder was similar if either a planar or a cylindrical source was used to estimate ε. Badawi et al. [8] examined the noise properties of NFs resulting from planar- or cylinder-derived ε, indicating that a planar source yields less noisy NFs.

In this work we compare the effect on reconstructed images of using either a uniform cylindrical phantom or a uniform low-scatter planar source to estimate ε in fully 3D PET. We examine the effect on radial-, axial-, and volume-uniformity as well as contrast recovery, and also examine residual geometric structure in ε. We investigate the effect of correcting the cylinder data for scatter prior to estimating ε, and results are compared for cylinder efficiency data which were corrected for geometric factors or not. We also investigate the effect of changing the width of the fan-beam used to construct the three-dimensional fan-beam for each detector.

II. METHODS

An elliptical uniform phantom (long axis=20cm, short axis=14cm) was used to compare normalization methods. This phantom was chosen since it represents a different geometry than the cylindrical phantom used to determine the detector efficiencies. The scans were acquired on a Siemens/CTI ECAT 953B scanner (detector block size 8x8, 2 block rings or 16 detector rings yielding 256 sinogram planes and 31 image planes, 384 detectors per ring, sinogram size 160 radial bins x 192 angular views) [9]. The image planes are numbered 1-31 in the text and figures. A high-statistics scan of the ellipse (1.3G total counts) acquired in 3D mode was scatter-corrected [10] and then normalized using five different sets of NFs, as described in Table 1. The normalized data were corrected for attenuation using identical measured attenuation correction factors and reconstructed with the Kinahan-Rogers algorithm [11]. A single scan of the ellipse was acquired in 2D mode for the sake of comparison. The 2D data were normalized using the standard software provided with the scanner, which does not incorporate geometric factors, and were then scaled to match the average value of the 3D data. Non-normalized 3D data were also analyzed to provide a reference point for the extent of the normalization corrections.

Table 1.

Description of components of Normalization Factors (NFs) used for reconstructions. "SC" indicates that the cylinder data were corrected for scatter prior to calculating the detector efficiency factors (ε).

Normalization Type	GF source	ε Source
2D	N/A	2D cylinder
3D plane	3D planar	3D planar
3D cylinder	3D planar	3D cylinder
3D cylinder SC	3D planar	3D cylinder, SC
3D cylinder NoGF	none	3D cylinder
3D cylinder SC NoGF	none	3D cylinder, SC
None	none	none

A. Radial Uniformity

The radial uniformity was examined by placing a series of 20 concentric annuli over the average of image planes 2-30 of the elliptical phantom. The annuli were centered in the image (not in the phantom) since the major artifacts related to normalization are ring-artifacts centered in the detector ring. The phantom was centered away from the center of the FOV to reduce the correlation between artifacts related to normalization and artifacts due to other factors such as scatter- and attenuation-correction, which tend to be centered in the phantom. The outer annuli do not form complete circles, since portions of the outer annuli were beyond the edge of the phantom and were excluded from the analysis. Our primary goal was to sample the phantom at discrete distances from the center of the FOV. Each annulus is ~2 pixels (4mm) wide. A Radial Uniformity Index (RUI) was calculated from an image averaged over planes 2-30 as:

$$RUI = (C(r)_{max} - C(r)_{min}) / C(r)_{avg} \quad (2)$$

where C(r) is the average concentration of a single annulus of average radius r, and the subscripts max, min, and avg denote, respectively, the maximum, minimum, and average concentrations for a set of 20 annuli.

B. Axial Uniformity

The axial uniformity was examined by placing a single large ROI on all planes 2-30 of the elliptical phantom. An Axial Uniformity Index (AUI) was calculated as:

$$AUI = (C(p)_{max} - C(p)_{min}) / C(p)_{avg} \quad (3)$$

where C(p) is the average concentration of a single plane p, and the subscripts max, min, and avg denote the maximum, minimum, and average concentrations, respectively, for a set of 29 planes. The AUI is a measure of the total range of the average planar concentrations. We use another index, the Axial Fractional Standard Deviation (AFSD) to compare the distribution of the planar averages:

$$AFSD = SD(C(p)) / C(p)_{avg} \quad (4)$$

where SD(C(p)) is the standard deviation of C(p). The AFSD is not as sensitive to outliers as the AUI.

The primary axial uniformity results were determined before the application of plane-to-plane calibration factors (derived by comparing ROI concentrations in each image plane of an elliptical phantom with the actual concentration as measured in a calibrated well-counter) to the image data. A secondary set of RUI, AUI, and AFSD was calculated after calibration factors were applied to each plane, in order to investigate how this quantification step might alter the uniformity results for the various normalization methods.

C. Image Volume Uniformity

The effect of the various normalization methods on the uniformity of the image volume was evaluated using a NEMA-type analysis [12]. A 1cm x 1cm grid was placed within the elliptical phantom, and the concentration in the area defined by each grid element was determined for every plane except the two end-planes. The following values were calculated for the set of grid ROIs ($grid_i$), for each plane and for all planes together: the average, variance, standard deviation, and the Non-Uniformity indices NU_{min}, and NU_{max} :

$$NU_{min} = (grid_{avg} - grid_{min}) / grid_{avg} \quad (5)$$

$$NU_{max} = (grid_{max} - grid_{avg}) / grid_{avg} \quad (6)$$

where the subscripts max, min, and avg denote the maximum, minimum, and average concentrations, respectively, for each set of grid pixels. The values of NU_{min} and NU_{max} for individual planes are not presented here; for the purpose of examining the effect of various normalization methods, the values calculated for the entire volume are representative of the more complex patterns shown by individual planes.

The non-uniformity indices NU_{min} and NU_{max} select the regions with the lowest and highest concentrations in the entire image volume; they indicate the largest deviations but do not provide information about the distribution of the grid pixels. We use an index of image noise for all of the $1cm^2$ grid pixels, the Grid Fractional Standard Deviation (GFSD), calculated as:

$$GFSD = SD(grid) / grid_{avg} \quad (7)$$

where SD(grid) is the standard deviation of the grid pixels for an entire image volume, except the first and last planes.

D. Contrast Recovery

An elliptical phantom containing a hot-spot in a warm background was scanned (420M total counts). The hot-spot consisted of a glass sphere (2.8 cm ID) suspended near the center of the phantom. The actual concentrations in the hot-spot (H) and the background (BG) were determined by measuring samples from each compartment in a well counter. The ratio was estimated as H:BG=5.02. The ratio H:BG indicates the quantification accuracy of each normalization method independently of the calibration method used. ROIs were placed on the hot-spot in each of 7 adjacent planes. The ROIs were sized according to the volume of the sphere present in each plane. The background concentration was determined by placing ROIs on planes 2-30, excluding the region near the hot-spot. All pixels were weighted equally within the H or BG regions.

E. Lack of structure in detector efficiency factors

If all geometric dependencies or systematic variations are removed from the detector efficiencies, only random variation in ε should remain. We sum ε over each block position to create a sum-image which yields a map of the dependence of ε as a function of block position (b) and axial position (ring number R). This sum-image should not show any residual structure if the geometric dependencies have been removed. This issue becomes important when a different source geometry is used to measure the detector efficiencies than was used to determine the geometric factors.

F. Optimal width of Fan-Beam

The fan-beam used to calculate ε is characterized by the parameter k, which describes the number of radial bins on either side of the central LOR for a given detector. A wider fan-beam tends to include more LORs and provide a statistically superior estimation. The effect of the width of the fan-beam was investigated by using uniform cylinder data, either corrected or not for scatter, to produce fan-beams of three widths: k=19, which ensures that all LORs are well within the phantom boundaries; k=29, which attempts to use all LORs within the cylinder; and k=42, which ensures that all LORs within the cylinder are used. The case of k=29 may be sensitive to different positioning of the phantom from one scan to the next, while k=42 includes a large number of scattered events outside of the cylinder.

III. Results and Discussion

A. Radial Uniformity

Radial uniformity results are presented in Table 2 and Fig. 1.

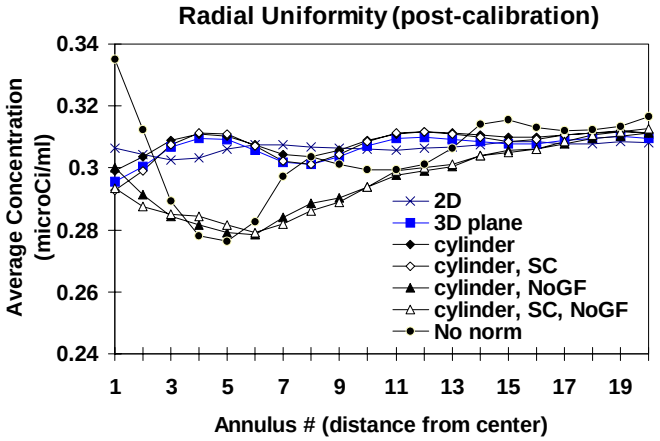

Figure 1: Radial uniformity for various normalization methods.

Detector efficiency factors derived from a cylinder and corrected with GFs obtained from a low-scatter plane-source ("3D cylinder") yield reconstructed images with a radial uniformity similar to that obtained if a plane-source is used to measure the detector efficiencies ("3D plane"). If the same cylinder data are not corrected with GFs ("...NoGF"), the radial uniformity becomes markedly worse. Correcting the cylinder data for scatter prior to calculating ε ("...SC") yields a small degradation in the radial uniformity.

Small differences in RUI between various types of normalization (compare 3D plane, 3D cyl, 3D cyl NoGF) depend heavily on the values of the central annulus (#1), which contains only ~13 pixels. The RUI measures the largest difference between all radial annuli in a single phantom and provides an objectve way to compare radial non-uniformities between phantom measurements; however, it can be sensitive to non-significant differences between single annulus values, particularly the central annulus. A comparison of the overall shape and magnitude of the radial uniformty plots in Fig. 1 indicates the radial uniformities of “3D plane”, “3D cyl” and “3D cyl NoGF” are very similar, as are the two radial uniformities of the “...NoGF” methods.

The radial non-uniformities evident in the 3D scans are attributed to the scatter-correction algorithm subtracting non-normalized scattered events.

Table 2. Results from radial and axial uniformity analysis. The indices RUI, AUI, and AFSD are defined in Equations 2-4.

Norm Type	RUI	AUI	AFSD
2D	0.0200	0.0290	0.0078
3D plane	0.0481	0.0544	0.0171
3D cyl	0.0407	0.0984	0.0340
3D cyl SC	0.0630	0.0991	0.0322
3D cyl NoGF	0.1106	0.0885	0.0305
3D cyl SC NoGF	0.1138	0.0816	0.0279
None	0.1947	0.1781	0.0392

B. Axial Uniformity

Axial uniformity results are shown in Table 2 and Fig. 2. The 2D method yields the best axial uniformity, followed by the fully planar method ("3D plane"). Axial uniformity is slightly worse for the uniform cylinder data.

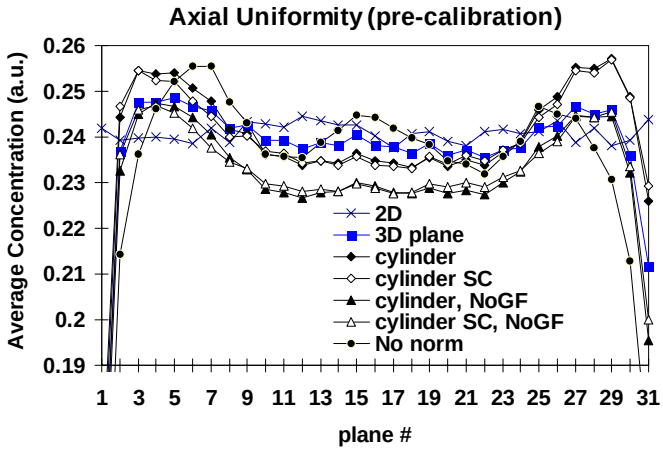

Figure 2: Axial uniformity for various normalization methods.

Normalization factors from GF-corrected cylinder data ("cylinder" and "cylinder SC") improve the axial uniformity compared to those cases where no GFs are used ("...NoGF"). Correcting the uniform cylinder data for scatter ("...SC") prior to estimating ε causes a slight improvement in axial uniformity.

C. Image Uniformity Results

The use of a cylinder instead of a plane-source for determining ε causes a slight increase in the non-uniformity of the reconstructed images. The non-uniformity results are summarized in Figures 3a,b. We also found (but do not present here) that the relative level of noise in the normalized sinograms follows the non-uniformity pattern shown for the reconstructed images.

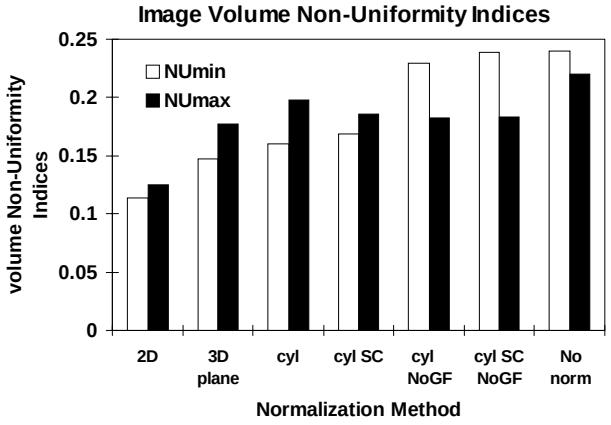

Figure 3a: Non-Uniformity Indices (NU_{min}, NU_{max}) for the entire phantom image volume (excluding the two end-planes) .

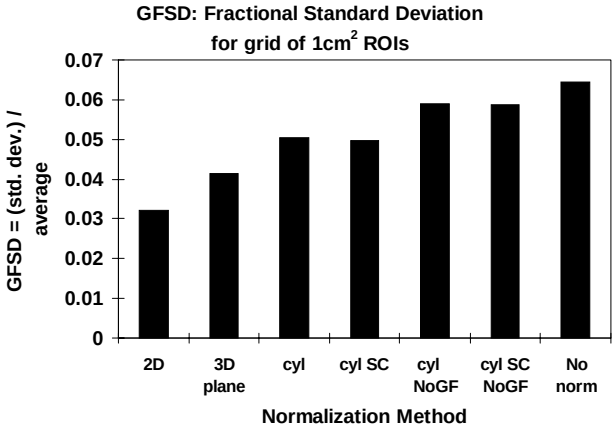

Figure 3b: Fractional standard deviation of grid (GFSD) of $1cm^2$ regions for phantom image volume (excluding the two end-planes).

Both the Non-Uniformity indices (Fig. 3a) and the GFSD index (Fig. 3b) indicate that using a uniform cylinder to determine detector efficiencies yields slightly less uniform images than use of a planar source. Correcting the cylinder for scatter prior to calculating the detector efficiencies has little effect on the non-uniformity (compare Fig. 3a,b "cyl" and "cyl SC"). If geometric corrections are not incorporated into the cylinder data, the resulting images are nearly as non-uniform as the case where no normalization was performed.

D. Contrast Recovery

The ability to recover the correct contrast between a hot and a warm region is similar if either a uniform cylinder or a plane-source is used to measure detector efficiencies. The ratio H:BG determined from placing ROIs on the image data is divided by the measured ratio; a perfect recovery of the contrast would yield a value of 1.0 in the graph shown in Figure 4. Correcting the cylinder for scatter slightly increases the measured ratio. If the cylinder data are not corrected for geometric dependencies, the ratio is similar to the case of no normalization.

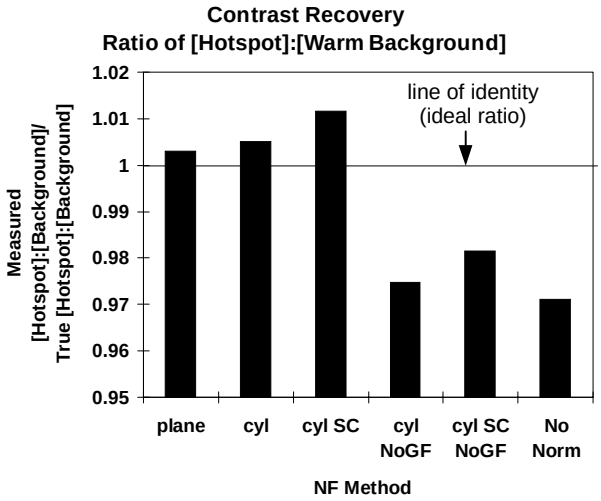

Figure 4: Contrast Recovery for various normalization methods.

E. Lack of structure in detector efficiency factors

If the cylinder data are not corrected for geometric dependencies, a large amount of residual structure remains and it may not be valid to evaluate ε from such a fan of LORs. The relative efficiencies of the detector crystals within a block if GF corrections are not applied can be clearly seen in Fig. 5, "3D cyl No GF" and "3D cyl SC No GF".

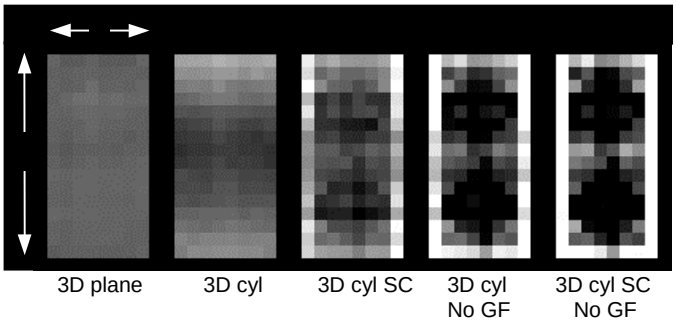

Figure 5: Geometric structure remaining in detector efficiency factors (ε). Individual detector efficiencies were summed for each block position (b) and Ring-number (R). All images are presented with the same grayscale.

If the cylinder data are corrected for scatter there is a relatively large residual block-structure apparent (Fig. 5, "3D cyl SC"). There is still some block-structure discernible in the plane-source normalization data ("3D plane"), but not as much as displayed by the cylinder data ("3D cyl"), which shows a decrease in ε for detectors from the central detector rings. This demonstrates that the detectors in the middle of the axial FOV receive more events if a cylinder is used to measure ε, since the distribution of scattered events is largest near the center of the FOV.

E. Optimal width of fan-beam

The radial uniformity results (Table 3) do not indicate a preference for any of the three fan-beam widths investigated. A slightly better axial uniformity results from using a smaller fan-beam width but the gain is quite modest. A slightly lower level of residual structure in the detector efficiency factors is obtained for k=29 than for narrower or wider fan-beams (data not shown). We favor k=19 because it yields the best axial uniformity, has a residual geometric structure comparable to the other widths considered, and can be expected to be less sensitive to differences in phantom placement than k=29, which corresponds to the edge of the 20cm phantom. Most of the results presented in this work used k=29. An analysis of the image non-uniformity (not shown) indicates that k=19 yields slightly more uniform images and k=42 yields slightly less uniform images than k=29, although the differences are small.

Table 3. Radial and Axial Uniformity Indices for various fan-beam widths (k) used to calculate ε.

Fan-beam	RUI	AUI	AFSD
k=19	0.0358	0.0963	0.0297
k=19, SC	0.0633	0.1017	0.0286
k=29	0.0400	0.0984	0.0340
k=29, SC	0.0622	0.0991	0.0322
k=42	0.0390	0.1108	0.0376
k=42, SC	0.0631	0.1109	0.0315

IV. CONCLUSIONS

Obtaining an accurate set of 3D PET normalization factors does not depend heavily on the source used to measure the detector efficiencies, but rather on the geometric factors used to correct the detector efficiency data. Use of a uniform cylinder to measure individual detector efficiencies (ε) can yield a level of image uniformity similar to that obtained through the use of a low-scatter uniform planar source, provided that an accurate set of geometric factors is used to correct the cylinder data. A cylinder source yields ε with a greater level of residual geometric structure. Use of a plane-source to measure ε yields slightly better image uniformity, but is impractical for routine use.

Correcting the cylinder data for scatter prior to estimating ε has a slightly degrading effect overall, although some individual figures of merit indicate small improvements to the reconstructed image data. The width of the fan-beam used to estimate ε has little effect on the resulting image uniformity or noise properties. A width which ensures that all LORs used to estimate ε are well within the cylinder boundaries will be less sensitive to small differences in phantom placement from one normalization scan to the next.

V. ACKNOWLEDGMENTS

This work was supported by a grant from the Canadian Medical Research Council and by a grant from the U.S. National Cancer Institute (F32-CA67486).

VI. REFERENCES

[1] Stazyk MW, Sossi V, Buckley KR, Ruth TJ, "Normalization measurements in septa-less PET scanners", *J. Nucl. Med*., vol 35 p.41P (abstract) 1994.

[2] Oakes TR, Sossi V and Ruth TJ, "Normalization for 3D PET with a low-scatter planar source and measured geometric factors", *Phys. Med. Biol*., (in press) 1998.

[3] Hoffman EJ, Guerrero TM, Germano G, Digby WM, Dahlbom M, "PET system calibrations and corrections for quantitative and spatially accurate images", *IEEE Trans. Nuc. Sci*. vol. 36(1) pp. 1108-1112, 1989.

[4] Ollinger JM, "Detector efficiency and Compton scatter in fully 3D PET", *IEEE Trans Nucl Sci*., vol. 42(4), 1168-73, 1995.

[5] Casey ME, Gadagker H, Newport D, "A component based method for normalization in volume PET" *Proc. Intl. Meeting on Fully Three-Dimensional Reconstruction in Radiology and Nuclear Medicine*, Aix-les-Bains, France, pp.67-71, 1995

[6] Bailey DL, Townsend DW, Kinahan P, Grootoonk S, Jones T, "An investigation of factors affecting detector and geometric correction in normalisation of 3-D PET data", *IEEE Trans. Nuc. Sci.*, vol. 43(6), pp. 3300-3307, 1996.

[7] Kinahan PE, Townsend DW, Bailey DL, Sashin D, Jadali F, Mintun M, "Efficiency Normalization techniques for 3D PET Data", *Proc. 1995 IEEE/MIC Conference*, 1995.

[8] Badawi RD, Lodge MA, Marsden PK, "Algorithms for calculating detector efficiency normalisation coefficients for true coincidences in 3D PET", *Phys. Med. Biol*., (in press) 1998.

[9] Spinks TJ, Jones T, Bailey DL, Townsend DW, Grootoonk S, Bloomfield PM, Gilardi M-C, Casey ME, Sipe B, Reed J, "Physical performance of a positron tomograph for brain imaging with retractable septa", *Phys.Med.Biol.*, 37:8, pp.1637-55, 1992.

[10] Bailey DL and Meikle SR, "A convolution-subtraction scatter correction method for 3D PET", *Phys. Med. Biol*., vol. 39, pp. 411-24, 1993.

[11] Kinahan PE and Rogers JG, "Analytic 3-D image reconstruction using all detected events", *IEEE Trans. Nucl. Sci*., vol. 36, pp. 964-968, 1989.

[12] Karp JS, Daube-Whitherspoon M, Hoffman EJ, Lewellen TK, Links JM, Wong W, et al, "Performance Standards in Positron Emission Tomography", *J.Nuc.Med.* vol.32,pp.2342-2350, 1991.